Disorder versus structure analysis in intergrowth urea inclusion compounds

2001 J. Phys.: Condens. Matter 13 1653

(http://iopscience.iop.org/0953-8984/13/8/304)

INSTITUTE OF PHYSICS PUBLISHING JOURNAL OF PHYSICS: CONDENSED MATTER

J. Phys.: Condens. Matter **13** (2001) 1653–1668 www.iop.org/Journals/cm PII: S0953-8984(01)14639-4

Disorder versus structure analysis in intergrowth urea inclusion compounds

P Rabiller[1], J Etrillard[1,2], L Toupet[1], J M Kiat[2,3], P Launois[4], V Petricek[5] and T Breczewski[6]

[1] Groupe Matière Condensée et Matériaux, UMR6626, Université de Rennes I, 35042 Rennes Cedex, France
[2] Laboratoire Léon Brillouin, CE Saclay, 91191 Gif-sur-Yvette, France
[3] Ecole Centrale Paris, Laboratoire Structures, Propriétés, Modélisation des Solides, UMR 8580, 92295 Châtenay-Malabry Cedex, France
[4] Laboratoire de Physique des Solides, UMR8502, bâtiment 510, Université Paris Sud, 91405 Orsay Cedex, France
[5] Institute of Physics, Academy of Sciences of the Czech Republic, Praha, Czech Republic
[6] Facultad de Ciencias, Universidad del Pais Vasco, Apdo 644, Bilbao, Spain

Received 12 June 2000, in final form 27 November 2000

Abstract

Alkane/urea inclusion compounds constitute a class of incommensurate composite materials, characterized by a pronounced one dimensional character and strong disorder of the alkane molecules. Intrinsic features of the alkane molecular form factor can be used to obtain a quantitative interpretation of the alkane subsystem translational degree of freedom whereas they lead to the restriction of observable Bragg reflections. A rigid body approach is also presented, which gives a simple description of the alkane sublattice modulation in the frame of (3 + 1) dimensional structure refinement.

1. Introduction

During the last few years, quasiperiodic structures, such as incommensurate modulated crystals, incommensurate composites and quasicrystals, have raised a great deal of interest. Incommensurate composite structures appear as quasiperiodic systems of intermediate complexity, since they consist of two interpenetrating and interacting sublattices with two mutually incommensurate periodicities in at least one direction [1]. Urea inclusion compounds constitute a family of molecular composite structures, where long chains of guest molecules, such as *n*-alkane, are embedded in parallel channels of the host urea sublattice (figure 1), which exhibit hexagonal symmetry [2]. The *n*-alkane arrangement along the channels' direction (denoted $\boldsymbol{c}_g$) is incommensurate with respect to the periodicity of the urea sublattice in this direction (denoted $\boldsymbol{c}_h$ and of about 11 Å). The approximately 5 Å size of the channel allows for rotation and translation disorder of the alkane molecules [3–5], which thus can accommodate the hexagonal symmetry of the composite. Many alkane urea inclusion compounds undergo a ferroelastic phase transition from hexagonal to orthorhombic symmetry with doubling of the cell and existence of domain structure [6–9]. Alkane molecules exhibit a herringbone-like arrangement in the low symmetry phase [7, 10] (figure 1), implying orientation ordering

0953-8984/01/081653+16$30.00

at the phase transition and pretransitional effects above transition temperature [4, 5]. As a consequence, diffraction patterns are very rich and complex and handling simultaneously disorder and structure refinement is a real challenge. Here we concentrate on the high temperature phase of the nonadecane/urea inclusion compound ($a = 8.22$ Å, $\boldsymbol{c}_h = 11.02$ Å and $\boldsymbol{c}_g = 26.36$ Å [6]).

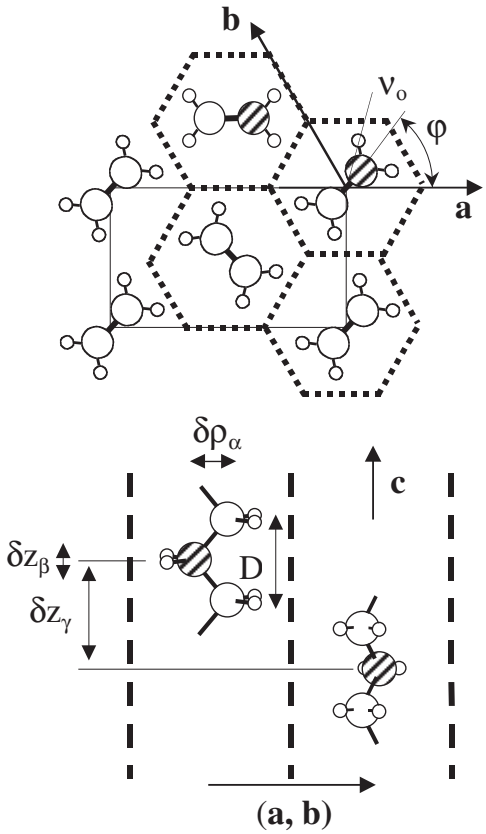

Figure 1. Schematic drawing illustrating the translational and orientational disorder of the alkane molecules inside the parallel channels built by the urea host sublattice. An orthorhombic cell showing the characteristic herringbone-like arrangement of the low temperature phase is displayed.

2. Experiment

Scattering experiments were carried out on single crystals of *n*-nonadecane/urea inclusion compound (denoted C19) prepared by slow evaporation of mixed solutions of urea and *n*-nonadecane in ethanol and isopropanol. Fully hydrogenated crystal ($0.8 \times 0.8 \times 2$ mm^3) was used for x-ray experiments and fully deuterated for neutrons ($4 \times 4 \times 4$ mm^3) in order to avoid large incoherent scattering of hydrogen. X-ray Bragg scattering data have been collected using a four-circle Enraf–Nonius CAD4 diffractometer with Mo Kα radiation (ω scans). A two-axis high resolution spectrometer developed at Ecole Centrale de Paris (ECP) with rotating anode Cu Kβ radiation has been used for precise measurements of a few reflection sets. Diffuse scattering was recorded on photographic films using an Enraf–Nonius precession

camera together with a Nitrogen Oxford Cryostat. The monochromatic Laue technique with imaging plates or photographic films was used under vacuum to get air scattering free diffuse scattering data. Studied intensity profiles have been extracted from the imaging plates and from digitized photographs. Neutron scattering was performed at the Laboratoire Léon Brillouin at the Orphée reactor (Saclay). Bragg scattering data were collected on a four-circle 6T2 diffractometer (thermal neutron guide, $\lambda = 1.54$ Å, ω, ω/θ or $\omega/2\theta$ scans according to apparatus resolution). Sollers windows have been used in order to increase the signal to noise ratio of the weaker or poorly resolved reflections. The structure refinement has been done from room temperature data using the program package JANA98 [11].

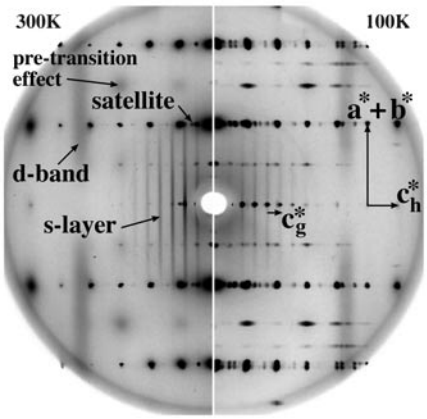

Figure 2. Zero level precession photograph (Cu Kα x-ray tube) in the ($\boldsymbol{a}^* + \boldsymbol{b}^*$, $\boldsymbol{c}^*$) equatorial plane above (left) and below (right) the phase transition holding at 160 K for the hydrogenated compound [6]. The $\boldsymbol{c}^*$ axis is displayed horizontally in the figure. Bragg spots at ($00l \neq 6n0$) positions are due to multiple scattering [13]. The ($11\bar{1}1$) satellite is pointed out close to the ($110\bar{1}$) alkane Bragg reflection.

3. Diffraction pattern

3.1. Bragg scattering

A cross section of the diffraction pattern of the composite structure obtained by precession technique is displayed in figure 2. A schematic diagram given in figure 3(b) illustrates the different contributions to the diffraction pattern, which consists of Bragg peaks on one hand and strong diffuse scattering on the other hand. The more intense Bragg peaks reflect the metric of the host urea sublattice (space group $P6_122$ on average), whereas weaker ones correspond to the guest alkane metric ($P622$) [12, 13]. Satellites at irrational location with respect to that of either host or guest subsystems definitely give a signature of the intermodulation of the two sublattices [14–16]. In the frame of superspace group theory [12], the Bragg reflections are classified as

- ($hkl0$) main host reflections from urea subsystem
- ($hk0m$) main guest reflections from the alkane subsystem
- ($hk00$) common reflections from both subsystems
- ($hklm$) l and m non zero, pure satellite reflections.

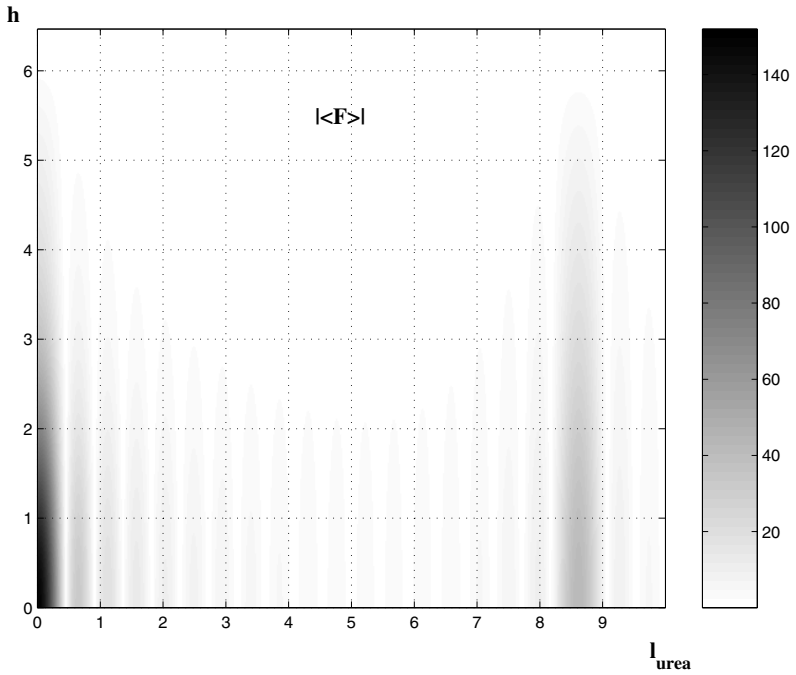

(a)

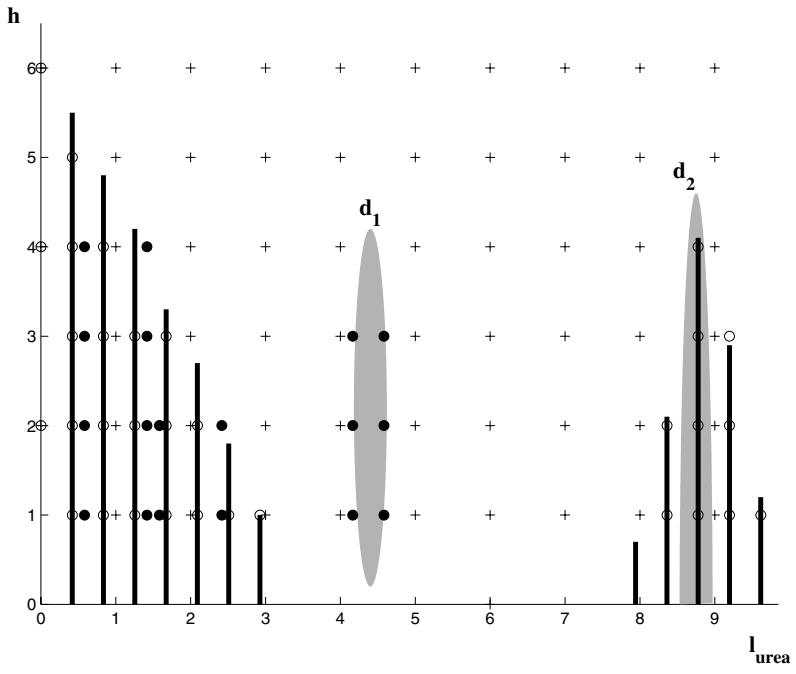

(b)

Figure 3. (a) Alkane molecular form factor in the (a^*, c^*) plane. (b) Schematic representation of Bragg, diffuse and satellite scattering: (+) urea reciprocal lattice nodes, (○) main alkane reflections, (|) s planes, (●) satellites. Diffuse d bands are shaded in grey.

The ($hkl0$) and ($hk0m$) reflections are in fact mixed main–satellite reflections: main reflection with respect to one sublattice and satellite for the other one.

3.2. Diffuse scattering

The diffuse scattering mainly consists of two distinct sets of parallel diffuse sheets perpendicular to the $\boldsymbol{c}$ direction [3–5]. One set is made of sharp layers (denoted s planes) [3] with a width (along the $\boldsymbol{c}$ direction) comparable to the Bragg resolution. They appear only close to the $m = 0$ reciprocal plane and superimpose on the ($hk0m$) Bragg levels. Their periodicity ($\boldsymbol{c}_g$) along the $\boldsymbol{c}$ direction is that of the alkane guest subsystem. This diffuse scattering is due to translational shift (δz_γ) of the alkane chains along the $\boldsymbol{c}$ direction from one channel to the others, which makes the diffraction pattern look like the Fourier transform of a one-dimensional (1D) system. Much broader layers (d bands) [3] appear on the scattering pattern at a distance which is the reciprocal of the internal periodicity (2.55 Å) of the $–CH_2–$ groups of the alkane molecules. Their width is consistent with the limited repetition of CH_2 entities over the finite length of alkane. Different models can be found in the literature [3–5] which interpret this scattering in terms of the single alkane molecular form factor. Maximum intensity is encountered on the $\boldsymbol{c}^*$ axis for even d-band orders whereas extinction is found on this same axis for odd orders, in consistency with half of the internal periodicity of the $–CH_2–$ groups when viewed in projection along the $\boldsymbol{c}$ axis (figure 3(a)). It might be noticed that no zero order d band can be seen in figure 2. Here we consider the alkane molecules as rigid bodies and divide the on-site alkane molecular disorder into translational disorder along the channel axis and rotational freedom around this axis. On-site translational disorder (δz_β) may occur since the geometrical length of the whole molecule (about 25 Å) is less than the 26.4 Å observed for the alkane sublattice periodicity ($\gamma = \boldsymbol{c}_g^*/\boldsymbol{c}_h^* = 0.418$) [14, 17].

4. Results and discussion

It is well known that thermal fluctuations destroy long range order in pure 1D systems [18, 19]. Such a behaviour applied to the alkane sublattice might lead to a quadratic increase of the s-plane width along the $\boldsymbol{c}^*$ direction. This phenomenon has been clearly observed recently by Weber *et al* by high resolution scattering on C14, C17 and C15/C16 mixture compounds using synchrotron x-ray radiation [20]. However since intermodulation satellites exist even far from the origin in the reciprocal space [6], one can argue that both intra-channel and inter-channel translational disorder may not completely prevent long range 3D spatial correlation. In this frame one can consider that the mean value of these disorders over all cells of the crystal might be close to zero whereas their quadratic fluctuations may be important. Furthermore it is clear from figure 2 that, in the case of C19 compound, both s planes and d bands are still present in the low symmetry phase—although some controversy about the existence of the d band in the low symmetry phase can be found in the literature [21]. The persistence of the s planes indicates that inter-channel translational disorder is not the driving force for the phase transition. Assuming that symmetry breaking is mainly related to orientational ordering of the alkane molecules (probably coupled to urea lattice shearing) [10, 22], we make the approximation of complete uncorrelation of translational and rotational parts of the alkane sublattice disorder.

At room temperature, diffuse scattering can be seen in figure 2 at Bragg positions corresponding to the orthorhombic symmetry of the urea sublattice, which are forbidden in the high temperature hexagonal symmetry. It is particularly strong for $h = k = n + 1/2$

and $l = 2p + 1$. This diffuse scattering, which condenses below the phase transition, can be interpreted as evidence of spatial correlation in the high temperature phase.

4.1. Structure factor models

In the frame defined above, simple models can be derived to obtain analytically the scattered intensity related to the alkane subsystem. These models, developed to describe some specific features of the diffuse scattering [23], can also be used to obtain quantitative information about translational disorder. Assuming there is no correlation between orientational and translational disorder, and treating alkane molecules as rigid bodies with their long axis parallel to the $\boldsymbol{c}$ axis, the scattered intensity can be written as the following average sum over all unit cells of the crystal:

$$I = \sum_{j,J} \exp[\mathrm{i}\boldsymbol{q}(\boldsymbol{r}_j - \boldsymbol{r}_{j+J})]\langle\exp[\mathrm{i}\boldsymbol{q}(\Delta\boldsymbol{r}_j - \Delta\boldsymbol{r}_{j+J})]\rangle\langle F_j F^*_{j+J}\rangle.$$

The F_j quantity represents the one-site molecular structure factor and depends only on the possible orientations of the alkane molecules. The $\boldsymbol{r}_j$ vector represents the position of the molecular centres of mass in the cell j. The translation fluctuation $\Delta\boldsymbol{r}$ is the sum of two terms, one representing on-site translation shift and a second taking into account the inter-channel shift. The second one is polarized along the $\boldsymbol{c}$ axis (δz_γ), whereas the first one can have components parallel (δz_β) and perpendicular ($\delta\rho_\alpha$) to the $\boldsymbol{c}$ axis. The latter is assumed with radial isotropy. The scattered intensity can be divided into four parts, denoting by W_β and W_γ the Debye–Waller-like factors $\{\langle\exp[iq_z\delta z_\beta]\rangle\langle\exp[\mathrm{i}q_\rho\delta\rho_\alpha]\rangle\}^2$ and $\langle\exp[\mathrm{i}q_Z\delta z_\gamma]\rangle^2$:

- Bragg:

$$I_{Bragg}(\boldsymbol{q}) \propto \sum \delta(\boldsymbol{G} - \boldsymbol{q}) W_\beta W_\gamma |\langle F\rangle|^2$$

  ($\boldsymbol{G}$ runs through reciprocal guest lattice vectors)
- s-plane:

$$I_{s\text{-}plane}(m) \propto \sum \delta(n - m) W_\beta (1 - W_\gamma) |\langle F\rangle|^2$$

  (n runs through non-zero integer numbers)
- diffuse:

$$I_{d\text{-}trans}(\boldsymbol{q}) \propto (1 - W_\beta)|\langle F\rangle|^2 \qquad \text{due to on-site translation disorder}$$

- diffuse:

$$I_{d\text{-}rot}(\boldsymbol{q}) \propto \langle F F^*\rangle - |\langle F\rangle|^2 \qquad \text{due to orientation disorder.}$$

Only the first three terms, which depend on the modulus of the average on-site structure factor, are considered here. Cylindrical coordinates are used with the z direction along the crystallographic $\boldsymbol{c}$ axis. A reciprocal space vector $\boldsymbol{q}$ is represented by (q_ρ, ψ, q_z) and a direct space vector $\boldsymbol{r}$ by (ρ, φ, z). W_β and W_γ are the pseudo-Debye–Waller factors $\{\langle\exp[\mathrm{i}q_z\delta z_\alpha]\rangle\langle\exp[\mathrm{i}q_\rho\delta\rho_\alpha]\rangle\}^2$ and $\langle\exp[\mathrm{i}q_Z\delta z_\gamma]\rangle^2$. Assuming Gaussian distributions for simplicity, these expressions become $W_\beta = \exp[-U_{z\beta}q_z^2 - U_{\rho\beta}q_\rho^2]$ and respectively $W_\gamma = \exp[-U_{z\gamma}q_z^2]$, where the U represents the mean square displacements. In the high temperature phase the distribution of angular positions was thought of as nearly free rotation [24] or statistically distributed jumps over six-fold discrete positions [25]: $\varphi_n = \varphi_0 + n(2\pi/6)$. Since these models lead to the existence of a zero order d band, which is not present in the diffraction patterns, it is necessary to bring in modifications [23]. For the present purpose only the case of homogeneously distributed domains with the herringbone-like arrangement is considered since it can be viewed as a crude limiting case of what can happen from the orientational ordering

point of view. In this model an orthorhombic cell is considered with metric corresponding to the high temperature hexagonal cell and only Bragg reflections belonging to the hexagonal symmetry are retained. The overall intensity is obtained by averaging over the domain orientations $2\pi/3$ apart. The F quantity can be written according to the possible orientations φ_n, using Bessel formalism [26]. The atomic scattering factors for carbon and hydrogen are denoted f_C and f_H respectively. The angular position (φ_n is that of carbon atoms and those of hydrogen atoms are $\varphi_n \pm \nu_0$ (figure 1). N is the number of carbon atoms in a molecule and the end methyl groups are considered as CH_2 entities. The internal periodicity of the alkane molecule is denoted D. Then for orientation φ_n, the one-site structure factor takes the form

$$F_n = S(\Omega)\left\{A(0) + 2\sum_{k_{even}>0}(-1)^{k/2}A(k)\right\} + 2S\left(\Omega + \frac{\pi}{2}\right)\mathrm{i}^N \sum_{K_{odd}>0}(-1)^{(k-1)/2}A(k)$$

$$S(\Omega) = \frac{\sin(N\Omega)}{\sin(\Omega)} \qquad \text{with} \qquad \Omega = q_z\frac{D}{4}$$

$$A(k) = \cos[k(\varphi_n - \psi)]\{f_C J_k(q_\rho \rho_C) + 2f_H \cos(k\nu_0) J_k(q_\rho \rho_H)\}.$$

It can be shown [23] that the average form factor $\langle F\rangle$ depends only on $S(\Omega)$ and even orders of $A(k)$. Then the translation part of diffuse scattering $(1 - W_\beta)|\langle F\rangle|^2$, will be important only on even orders of the d bands ($q_z = n4\pi/D$) where $S(\Omega)$ is a maximum (figure 4(a)).

4.2. s-plane profiles

Close to the $\boldsymbol{c}^*$ axis, the radial terms $q_\rho\rho_C$ and $q_\rho\rho_H$ are close to zero and only the zero order Bessel function is meaningful. The structure factor then approximately goes like $F(q_z) = S(q_z)\{f_C(q_z) + 2f_H(q_z)\}$. This can be used to obtain quantitative information about $U_{z\beta}$ and $U_{z\gamma}$. An illustration is given in figure 4 where q_z is given in the guest subsystem relative units. The $W_\beta(1 - W_\gamma)$ function (figure 4(b) heavy line) shows a maximum function moving towards higher m values when reducing the $U_{z\gamma}$ value from infinity (purely 1D system) to smaller values (3D long range order). This causes a significant intensity reduction of the first two s planes in good agreement with experimental x-ray observation reported in figure 5 and neutron diffuse scattering [6]. Increasing the $U_{z\beta}$ term causes an intensity reduction of the s planes close to the second d layer. It is in fact necessary to assume a value of at least 0.2 to 0.3 Å^2 for $U_{z\beta}$ to make s-plane contribution negligible compared to that of translation diffuse scattering. Figure 4(c) represents the resulting effect of $U_{z\beta}$ and $U_{z\gamma}$ terms on the s-plane profiles when the experimental resolution is introduced ($\sigma_m = 0.11\ m$ units).

An experimental x-ray profile, extracted from a monochromatic Laue photograph, is shown in figure 5. Profile refinement is done after Lorentz correction is applied to experimental data. The background is represented by an order two q_z polynomial. The s-plane contribution is the convolution of a Gaussian resolution function and a sum of Lorentzian functions [26] located at multiple values of $\boldsymbol{c}_g^*$ (m up to 6). The resolution function width is determined from weak Bragg reflections and kept constant ($\sigma_m = 0.11\ m$ units). When allowed to vary, the quadratic increase of the Lorentzian width remains far within the resolution and has been considered meaningless. The individual root mean square displacement $\delta_{z\beta} = (U_{z\beta})^{0.5} = 0.45 \pm 0.25$ Å is compatible with the difference between alkane geometrical length (about 25 Å) and alkane subsystem periodicity (26.4 Å). On the other hand the inter-channel shift $\delta_{z\gamma} = (U_{z\gamma})^{0.5} = 1.9 \pm 0.1$ Å is close to one-sixth of the urea periodicity (1.84 Å) characteristic of the host lattice helix.

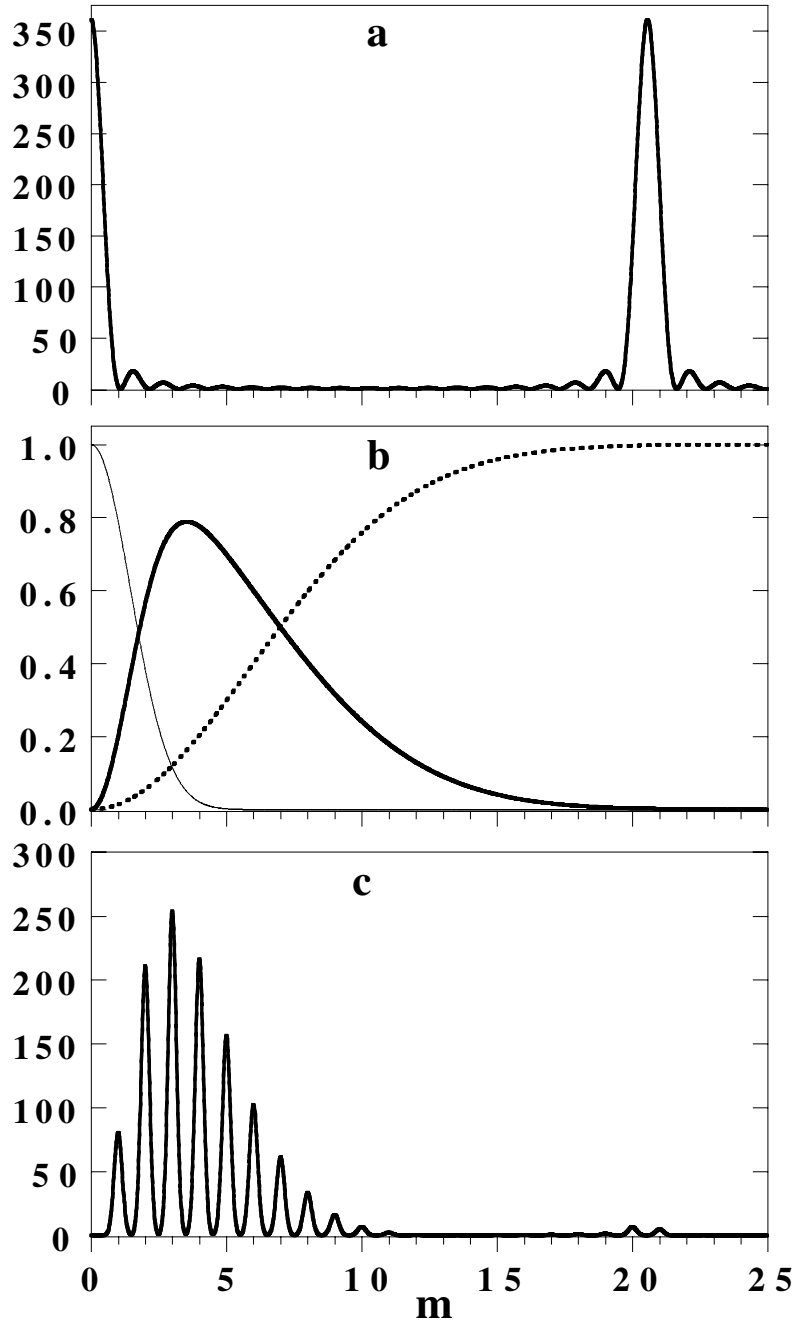

Figure 4. (a) Characteristic function $|S(q_z)|^2$ representing the limitation of the internal periodicity to the alkane molecular length along the c axis. Relative alkane reciprocal units are used. (b) Dampening functions for s plane scattering $W_\beta(1 - W_\gamma)$ (heavy line), translational diffuse scattering $(1 - W_\beta)$ (dotted line) and Bragg scattering $W_\beta W_\gamma$ (thin line). (c) s-plane profile resulting from experimental values of W_β, W_γ and resolution.

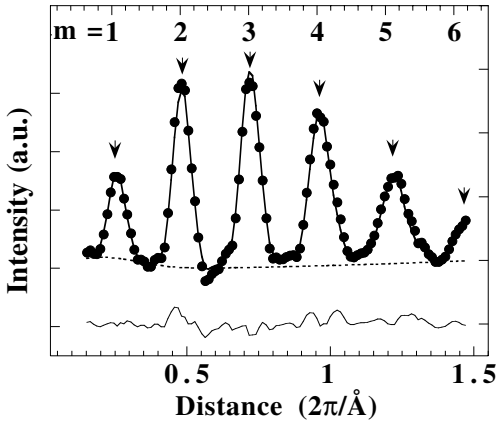

Figure 5. X-ray s-plane profile along the c^* axis. The length of the perpendicular component in the (a^*, b^*) plane q_ρ is slightly less than 0.3 $|a^*|$. The lower curve shows the residual between calculated and observed data. The final reliability R factor is less than 2%.

4.3. Accuracy of measured alkane Bragg reflections and intermodulation satellites

The combination of the $S(\Omega)$ function and mean square displacement along the c axis appearing in the damping function $W_\beta W_\gamma$ of the Bragg reflections makes these almost unobservable over $m = 3$ (figures 3 and 4(b) thin line). For this limited set, the measured intensity is biased by the s-plane contribution. Contamination by the s plane depends on the relative crystal orientation—the so-called ψ scan. As an example, fluctuations of about 15% are observed for (1001) and equivalent reflections. A simulation of the ψ-angle effect based on solely geometric considerations is given in figure 6 for the (2203) reflection. Peak profiles are obtained for ω-scans assuming that the intensity for a Bragg reflection or an s plane, at an ω-value has a Gaussian dependence on the distance from the Ewald sphere to the considered position in the reciprocal network at that ω-value. The anisotropy of the resolution perpendicular to the equatorial plane of Ewald sphere is taken into account with the factor of 1.5. The s-plane weight has been arbitrarily chosen equal to 10% of the ($hk0m$) considered reflection and for simplicity structure factors are assumed constant throughout the scan. The result of the simulation is displayed in figure 6. The origin of the ψ-angle is chosen such that the integrated intensity is equal to that of the ($hk0m$) alone. This situation corresponds to the associated s-plane nearly parallel to the equatorial plane, yielding a nearly constant contribution, which can easily be subtracted for integration purposes. For ψ-angle about 90° the s plane is nearly perpendicular to the equatorial plane and its contribution the same width as the Bragg peak and both are centred at the same ω-value. One then retrieves the expected 10% increase. For a ψ-angle about 30° the s-plane contribution slightly enlarges the bottom of the peak profile and gives the maximum effect on the integrated intensity. In the case where the s-plane would be close to a satellite or a weak urea Bragg peak, its contribution would be weaker since the distance from the plane to the Ewald sphere would be greater. But if not negligible, it would not be centred at the same ω-value and its effect would appear as giving a slope to the background, thus having little consequence to the integrated intensity. Another contamination which biases or masks the alkane Bragg peak or satellites is the one of diffuse scattering appearing at the bottom of strong common or urea Bragg peaks. This scattering appears along the c^* direction as well as in the plane parallel to (a^*, b^*) preferentially in directions $\pm a^* \pm b^*$. It has a Lorentzian shape with a width of about 0.2 to 0.3 relative units as illustrated in figure 7 for

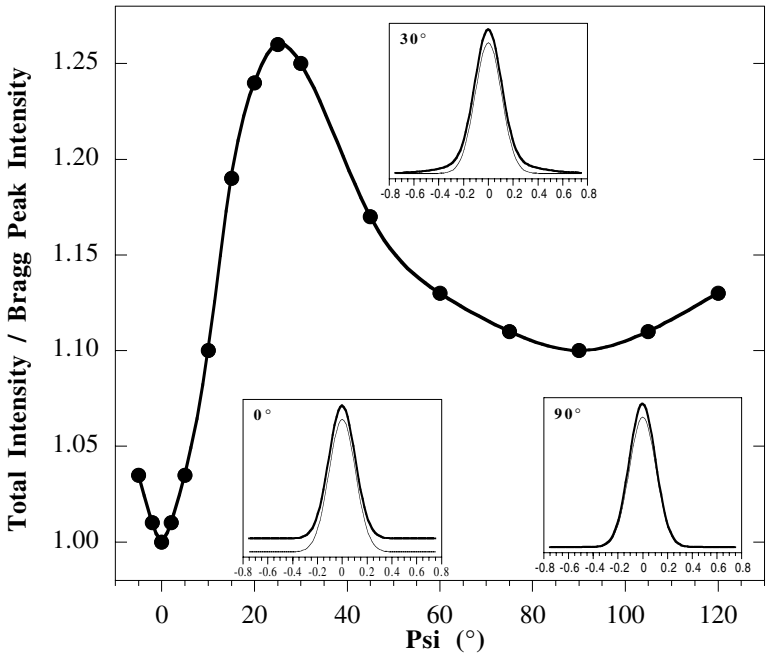

Figure 6. Simulation of ψ-scan effect on the measured intensity corresponding to ($hk0m$) alkane Bragg peak superimposed on the mth order s plane. The presented case corresponds to (2203). The Bragg peak profile has a Gaussian shape with width corresponding to the observed one (half width 0.08°). Profiles are shown for $\psi = 0°$, 30° and 90°, which correspond to situations detailed in the text. The weight of s-plane scattering has been taken arbitrarily to 10% of that of Bragg scattering.

the (5000) common reflection. Since urea Bragg peak intensities are on average two to three orders of magnitude greater than alkane Bragg peaks and satellites, this diffuse scattering contamination often leads to the rejection of these latter scattering reflections. Another aspect is the limitation in indexing accuracy. Within the experimental resolution it is not possible to discriminate for instance the ($hk011$) reflection from the ($hk5\bar{1}$) reflection.

4.4. Superspace refinement

Owing to the preceding limitations, only ($hk01$) alkane reflections and ($hklm = \pm 1$) satellites can be included together with ($hkl0$) urea reflections to perform superspace refinement. Furthermore only the discrete six-fold model can be put in the program package JANA98 to satisfy $P622$ symmetry. Figure 8 displays the calculated and observed ($hk01$) x-ray structure factors as a function of Bragg angle. There is almost no difference between the six jump and free rotation models in the experimental range due to the predominance of the zero order Bessel function and atomic form factor decay (figure 8(a)). The discrepancy that could be expected for the hypothetical herringbone model becomes appreciable only for weak structure factors and great experimental errors (CAD4 data in figure 8(b)). Measurements made manually on a few data with the high resolution ECP spectrometer suggests that CAD4 weak structure factors may be overestimated. It is also necessary to invoke a transverse root mean square displacement $\delta\rho_\alpha$ of about 0.3 Å to make the six-fold model fit with ECP data, in good agreement with the value proposed by Welberry *et al* from Monte Carlo simulation [27].

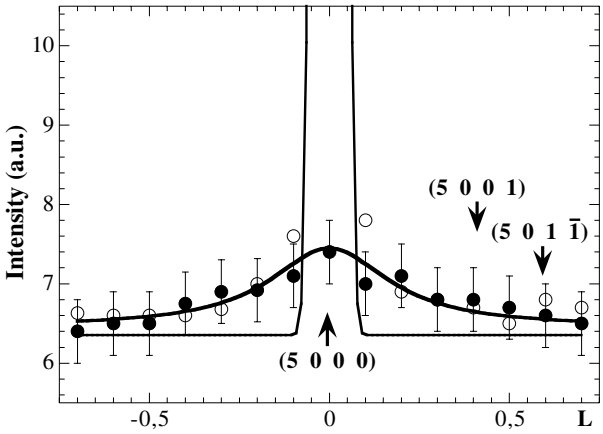

Figure 7. Analysis of diffuse scattering at the bottom of the strong common (5000) reflection (○). The thin line correspond to a Gaussian contribution (half width 0.03 relative units). Another scan is done at $h = 4.8$ (● and broad line). This enables us to fit the diffuse scattering with a Lorentzian with half width of about 0.2 relative units.

Table 1. Reliability factors[a] for the (3 + 1) superspace structure refinement of a *n*-nonadecane/urea crystal.

Total (all): independent reflections	X-ray[b] $C_{19}H_{40}$/urea-h4			Neutron[c] $C_{19}D_{40}$/urea-d4		
Criterion for observed (obs) reflections ($I > 3\sigma(I)$)	Total (obs)	R_{all}	R_{obs}	Total (obs)	R_{all}	R_{obs}
Main host reflections	313	0.0449	0.0397	263	0.3648	0.2982
($hkl0$)	(285)			(157)		
Main guest reflections	50	0.9448	0.2800	18		
($hk0m$); $m = 1$	(12)			(18)		
Common main reflections ($hk00$)	31	0.0614	0.0579	23	0.2768	0.2396
	(26)			(16)		
Satellite reflections	631	1.4681	0.4228	7		
($hklm$); $m = -1, 1$	(11)			(7)		

[a] Given R factors are defined as $R = \sum w(|F_{obs}| - |F_{calc}|)^2 / \sum w|F_{obs}|^2$ with $w = (1/\sigma(F_{obs}))^2$.
[b] The composite structure has been refined in (3 + 1) dimensional space (JANA98).
[c] The non-modulated three dimensional host structure has been refined in a conventional way, i.e. only ($hkl0$) and ($hk00$) reflections have been taken into account.

The structure of the incommensurate composite crystal *n*-heptadecane($C_{17}H_{36}$)/urea-h4 has been previously studied by Weber *et al* from x-ray diffraction at room temperature [15]. This (3 + 1) dimensional refinement investigation—with space group $P6122(00\gamma)000$ [12]—suggests that the guest substructure is heavily modulated by the host one whereas the urea framework is non-modulated. The modulation is found to be strongly non-harmonic (harmonics up the fourth order) and to exhibit maxima at positions where –CH_2– groups are facing nitrogen atoms. In this structure refinement, the orientation of the alkane molecules within the urea channel (proposed by Smith [13]) is chosen such that the plane of the C–C bonds points towards the sides of the hexagonal tunnel cross-section.

In the present study, the urea sublattice is refined using ($hkl0$) and ($hk00$) reflections for both x-ray and neutron data and treating urea molecules as rigid bodies. It seems reasonable

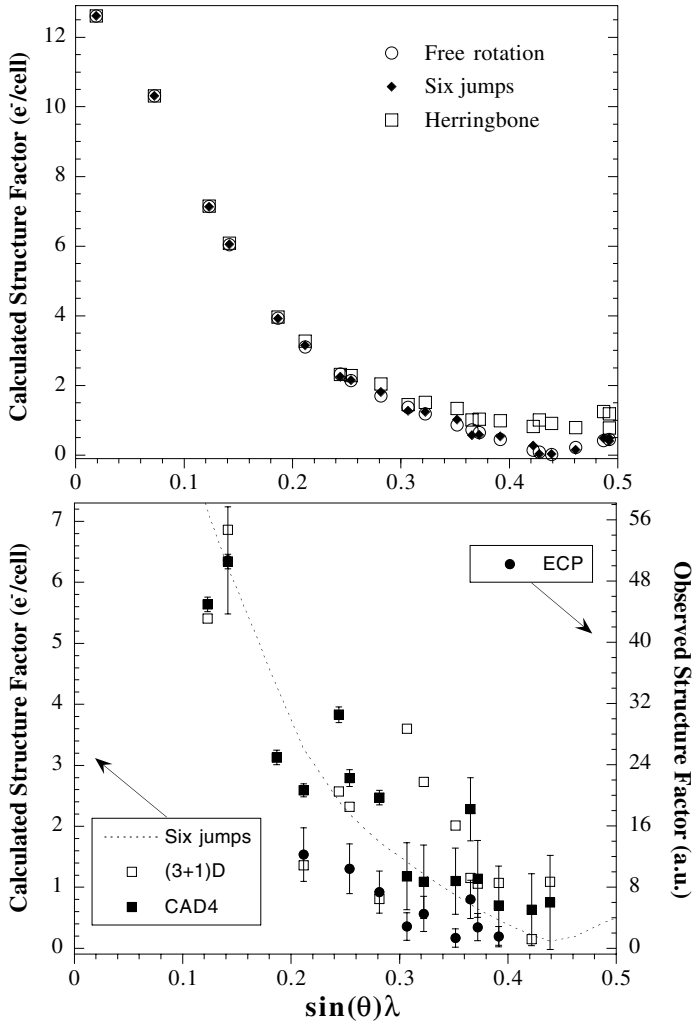

Figure 8. (a) X-ray structure factors of ($hk01$) reflections as a function of Bragg angle derived from models: six-fold jump model (♦), free rotation (○) and herringbone-like arrangement (□); (b) comparison of calculated and observed x-ray structure factors: (□) (3+1)D JANA98 refinement results, (■) CAD4 four-circle Nonius diffractometer data set and (●) ECP high resolution two-axis spectrometer data set. The six jumps model is given as a guide (dotted line).

from the disorder analysis to use as well a rigid body approach for the alkane (stretched all-*trans* conformation) with the six-fold position model and only one harmonics. This limits the number of adjustable parameters and prevents from giving too much significance to deformation of the alkane molecule at the atomic scale. The most complete collected data set was obtained from CAD4 x-ray measurements. Increase of the host scattering weight was expected by using neutron scattering from deuterated sample since in that case the ratio $F^{urea}_{(000)}/F^{alkane}_{(000)}$ is increased by a factor of about 4.5. The expected improvement is counterbalanced by lower counting statistics and bad resolution (increase of diffuse scattering contamination). Particularly, since a different scale factor has to be applied for reflections collected with Sollers windows, only main Bragg reflections of each subsystem could be refined separately. The refinement conditions

Table 2. Modulation parameters in subblattices coordinate system.

Urea				Alkane			
Translation (fractional units)		Rotation (dimensionless)		Translation		Rotation	
$\boldsymbol{u}_t^s$	$\boldsymbol{u}_t^c$	$\boldsymbol{u}_r^s$	$\boldsymbol{u}_r^c$	$\boldsymbol{u}_t^s$	$\boldsymbol{u}_t^c$	$\boldsymbol{u}_r^s$	$\boldsymbol{u}_r^c$
0.0059(9)	0.0012(2)	0.0018(3)	−0.0045(5)	0.0028(4)	0.0049(7)	−0.0033(5)	−0.0057(9)
0.0000	0.0024(4)	0.0000	−0.009(1)	0.0056(9)	0.0000	−0.0066(10)	0.0000
−0.0012(2)	0.000	−0.0022(4)	0.0000	0.0000	0.0000	0.0000	0.0000

and final reliability factors are listed in table 1. With this simple approach, good values of the reliability factors are obtained for urea and common reflections whereas much higher values are found for alkane and satellite reflections. Those are nevertheless practically equivalent to the published ones (see table 6 in [15]). The modulation is given by two vectors, which define the orientation and displacement of a single molecule around its centre of mass $\boldsymbol{R}$ according to

$$\boldsymbol{u} = \boldsymbol{u}_t + \boldsymbol{u}_r \times (\boldsymbol{r} - \boldsymbol{R})$$

where $\boldsymbol{r}$ represents the individual atomic position. In this expression, valid for small angular displacements, the translation and rotation parts, $\boldsymbol{u}_t$, respectively $\boldsymbol{u}_r$, can be decomposed in sine and cosine terms with $\boldsymbol{q}_c$ the modulation vector:

$$\boldsymbol{u}_t = \boldsymbol{u}_t^s \sin(\boldsymbol{q}_c \cdot \boldsymbol{R}) + \boldsymbol{u}_t^c \cos(\boldsymbol{q}_c \cdot \boldsymbol{R})$$
$$\boldsymbol{u}_r = \boldsymbol{u}_t^s \sin(\boldsymbol{q}_c \cdot \boldsymbol{R}) + \boldsymbol{u}_r^c \cos(\boldsymbol{q}_c \cdot \boldsymbol{R}).$$

The resulting parameters satisfying symmetry constraints for both urea and alkane subsystems are given in table 2. The modulation is found to be weak for the urea framework in agreement with the literature [15]. Concerning the alkane, the modulation only significantly affects the orientation of alkane molecules. On one hand this is not surprising from the restricted set of $(hk0m)$ included in the refinement process. On the other hand it is in agreement with the observation of satellites in the region close to the first d band, where the average molecular form factor of alkane is close to zero. It can be shown [6] that, in the case of a one harmonic modulation function, satellite structure factors are proportional to the structure factors of both average subblattices. If one of them is very weak, the pure modulation effect must be important. On the other hand, the first d band corresponds essentially to orientational disorder of alkane molecules [23]. The fact that the initial orientation of alkane molecules is chosen randomly and that the refinement process converges is an indication of the stability of the process.

No significant amount of translational modulation is needed. Individual atomic temperature parameters—constrained to be equal for all atoms—converge to 0.12 ± 0.02 Å for the isotropic root mean square displacement. This value is much less than those obtained for the translational shifts ($\delta_{z\beta} = 0.45$ Å and $\delta z_\gamma = 1.9$ Å) and transverse displacement ($\delta\rho_\alpha \sim 0.3$ Å) deduced from ECP diffraction data. The difficulty to describe translational disorder is certainly one reason for the high R-factors observed for the alkane and satellite parts. Refining with anisotropic thermal displacements does not give better a result. When kept constant with high values along the c-axis (even up to 10 Å), no improvement in the reliability factor is obtained. On the other hand, allowing refinement of the z-component of thermal parameters leads to divergence of the refinement process. In that case strong correlation is found between modulation parameters and thermal parameters, which would be minimized only if additional $(hk0m)$ alkane reflections could be included. Figures 9 and 10 give an illustration of the modulation in planes perpendicular and parallel to the modulation vector direction. The first interesting result concerns the orientation of the alkane molecules.

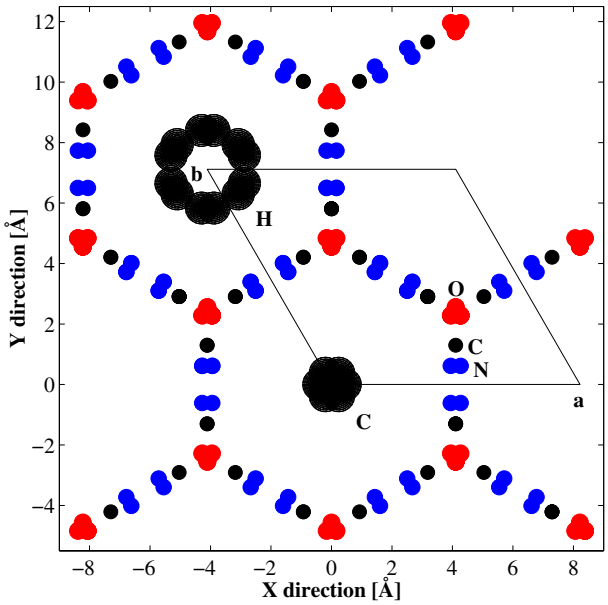

Figure 9. Illustration of the modulation in the ($\boldsymbol{a}$, $\boldsymbol{b}$) plane. View of the host and guest substructure projected along the [001] direction. Projection of 400 alkane molecules' carbon atoms is shown at the origin site whereas the corresponding hydrogen projection is displayed at the (0, 1) site of the hexagonal cell.

In figure 9 the projection, onto the ($\boldsymbol{a}$, $\boldsymbol{b}$) plane, of 400 alkane molecule carbon atoms is plotted at the (0, 0) site of the hexagonal cell. The corresponding projection of hydrogen atoms is plotted at the (0, 1) site. The mean value of carbon radial coordinate is 0.49 Å, very close to 0.43 Å, which is the value obtained for an alkane molecule with its long axis strictly parallel to the $\boldsymbol{c}$ axis. The associated quadratic fluctuation is 0.20 Å and compares well with the $\delta\rho_\alpha$ transverse displacement. A similar conclusion can be drawn for hydrogen atoms (mean radius 1.32 Å, quadratic fluctuation 0.22 Å). The carbon angular distribution is rather flat and remains within 20% from the mean uniform $1/2\pi$ distribution. The consequence of such a radial and angular distribution is that the outermost hydrogen atoms can approach the urea channel walls and may interact with oxygen or nitrogen atoms of neighbouring urea molecules. This is shown in figure 10, which represents a cross section in the plane ($2\boldsymbol{a} + \boldsymbol{b}$, $\boldsymbol{c}$). Only the projection of the outermost hydrogen atoms and the closest urea molecules are plotted. The smallest intermolecular distance corresponds to an H...N distance of about 2.2 Å. As in [15], the maximum of the modulation amplitude is about 0.5 Å and is obtained close to the nitrogen atoms pointing inside the tunnel. The minimum H...O distance is about 3 Å, too long to correspond to usual hydrogen bonding [28].

5. Conclusion

It has been shown that complementary information can be obtained from diffuse and Bragg scattering concerning the structure of nonadecane/urea inclusion compounds. The peculiar shape of the guest (alkane) molecular form factor allows quantitative interpretation of the translational disorder of the guest molecules. A simple (3+1) dimensional composite structure has nevertheless been proposed using rigid body approach for both host and guest's frameworks.

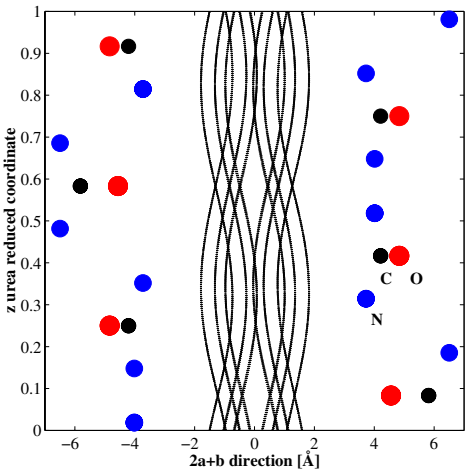

Figure 10. Side view of the alkane modulation in the $(2\boldsymbol{a}+\boldsymbol{b}, \boldsymbol{c})$ plane. Only the projection of the outermost hydrogen atoms and closest urea molecules is shown. Urea subsystem fractional units are used on the vertical axis.

The characteristic feature of the alkane form factor and the presence of disorder makes the number of experimentally accessible structure factors very limited for the alkane part. The refinement process is stable but fails in describing correctly the translational disorder of the guest sublattice. The urea framework is almost rigid whereas alkane is strongly disordered as in the case of Hg/AsF_6 compound [29]. This can explain the correlation between modulation and thermal parameters appearing in the refinement process as well as the high R-factors for the alkane and satellite reflections. The main contribution to the modulation function is the rotational part of alkane molecules. This enables alkane hydrogen atoms to approach significantly the urea tunnel walls. Although this is consistent with the idea of mutual interaction between both sublattices, it does not bring additional information about the nature of the interaction. One can eventually ask if concomitant and accurate analysis of disorder and modulation can ever be reached, in the high temperature phase, as well as in the low temperature phase where the domain structure complexity may largely overpass the intensity gain of guest and satellite reflections. Complementary information then come from the field of dynamical investigations [6, 30, 31].

Acknowledgments

The authors wish to thank the following persons for fruitful and stimulating discussions: Dr T Weber (Laboratorium Für Kristallographie, Universität Bern), Professor H Boysen (Institut Für Kristallographie Der Universität, München), Dr R Moret (LPS, Université Paris-Sud), Dr B Toudic (GMCM, Université de Rennes 1) and Dr F Guillaume (Laboratoire de Physico-Chimie Moléculaire, Université de Bordeaux I).

References

[1] Janssen T and Janner A 1987 *Adv. Phys.* **36** 519
[2] Hollingsworth M D and Harris K D M 1996 *Comprehensive Supramolecular Chemistry* vol 6 (Oxford: Pergamon) p 177

[3] Forst R, Jagodzinski H, Boysen H and Frey F 1987 *Acta Crystallogr.* B **43** 187
[4] Fukao K 1994 *J. Chem. Phys.* **101** 7882
[5] Fukao K 1994 *J. Chem. Phys.* **101** 7893
[6] Lefort R 1998 *PhD Thesis* Université Rennes I
[7] Forst R, Boysen H, Frey F and Jagodsinski H 1986 *J. Phys. Chem. Solids* **47** 1089
[8] Chatani Y, Anraku H and Taki Y 1978 *Mol. Cryst. Liq. Cryst.* **48** 219
[9] Forst R, Jagodzinski H, Boysen H and Frey F 1990 *Acta. Crystallogr.* B **46** 70
[10] Lynden-Bell R M 1993 *Mol. Phys.* **79** 313
[11] Petricek V and Dusek M *JANA98 Programs for Modulated and Composite Crystals*
[12] van Smaalen S and Harris K D M 1996 *Proc. R. Soc.* A **152** 677
[13] Smith A E 1952 *Acta Crystallogr.* **5** 224
[14] Lefort R, Etrillard J, Toudic B, Guillaume F, Breczewski T and Bourges P 1996 *Phys. Rev. Lett.* **77** 4027
[15] Weber T, Boysen H, Frey F and Neder R B 1997 *Acta Crystallogr.* B **53** 544
[16] Weber T, Boysen H, Honal M, Frey F and Neder R B 1996 *Z. Kristallogr.* **211** 238
[17] Harris K D M and Thomas J M 1990 *Trans. Faraday Soc.* **86** 2985
[18] Vainshtein B K 1966 *Diffusion of X-rays by Chains Molecules* (Amsterdam: Elsevier)
[19] Emery V J and Axe J D 1978 *Phys. Rev. Lett.* **40** 1507
[20] Weber T, Boysen H and Frey F 2000 *Acta. Crystallogr.* B **56** 132
[21] Weber T 1997 *PhD Thesis* München
[22] Yeo L and Harris K D M 1997 *Acta Crystallogr.* B **53** 822
[23] Rabiller P *et al* in preparation
[24] Greenfield M S, Vold R L and Vold R R 1985 *J. Chem. Phys.* **83** 1440
[25] Cho Y, Kobayashi M and Tadokoro H 1986 **84** 4636
[26] Jagodzinski H and Frey F 1993 *International Tables for Crystallography* vol B, ed U Shmueli for International Union of Crystallography (Dordrecht: Kluwer) ch 4.2
[27] Welberry T R and Mayo S C 1996 *J. Appl. Crystallogr.* **29** 353
[28] Espinosa E, Souhassou M, Lachekar H and Lecomte C 1999 *Acta Crystallogr.* B **55** 563
[29] Heilmann I, Axe J D, Hastings J M, Shirane G and Heeger A J 1979 *Phys. Rev.* B **20** 751
[30] Le Lann H 2000 *PhD Thesis* Université Rennes I
[31] Le Lann H, Odin C, Toudic B, Ameline J C, Gallier J, Guillaume F and Breczewski T 2000 *Phys. Rev.* B **62** 5442